

# UC Berkeley

## Recent Work

### Title

Clockwise Hysteresis Loops in the Macroscopic Fundamental Diagram

### Permalink

<https://escholarship.org/uc/item/2x98k1x2>

### Authors

Gayah, Vikash V.  
Daganzo, Carlos F.


### Publication Date

2010-09-01

# **Clockwise Hysteresis Loops in the Macroscopic Fundamental Diagram**

**Vikash V. Gayah and Carlos F. Daganzo**

WORKING PAPER  
UCB-ITS-VWP-2010-8

 UC Berkeley Center for Future Urban Transport  
A **VOLVO** Center of Excellence



**September 2010**

# Clockwise Hysteresis Loops in the Macroscopic Fundamental Diagram

WORKING PAPER

Vikash V. Gayah and Carlos F. Daganzo

UC Berkeley Center for Future Urban Transport,  
A Volvo Center of Excellence

September 27, 2010

## Abstract

A recent study reported that the Macroscopic Fundamental Diagram of a medium size city exhibited a clockwise hysteresis loop on a day in which a major disturbance caused many drivers to switch to unfamiliar routes. This paper shows that clockwise loops are to be expected when there are disturbances, especially if the disturbances cause a significant fraction of the drivers to not change routes adaptively. It is shown that when drivers are not adaptive networks are inherently more unstable as they recover from congestion than as they are loaded. In other words, during recovery congestion tends more strongly toward unevenness because very congested areas clear more slowly than less congested areas. Since it is known that uneven congestion distributions reduce network flows, it follows that lower network flows should arise during recovery, resulting in clockwise loops. Fortunately, in sufficient numbers, drivers that choose routes adaptively to avoid congested areas help to even out congestion during recovery, increasing flow. Thus, clockwise loops are less likely to occur when driver adaptivity is high.

# 1 Introduction

Investigations of the relationship between average flow and average density on an urban network have a long history. Godfrey (1969) appears to have been the first to propose that this relationship was unimodal. This idea was reintroduced several times (Herman and Prigogine, 1979; Ardekani and Herman, 1987; Mahmassani and Peeta, 1993; Olszewski et al., 1995), and most recently (Daganzo, 2007) as a part of an analytical model describing the dynamics of a traffic network. This last reference also proposed favorable conditions for such a relationship to exist. This idea was furthered in Daganzo and Geroliminis (2008) which showed theoretically that a reproducible relationship should arise if the traffic network meets a few regularity conditions. Using empirical data from the traffic network of Yokohama, Japan, which approximately meet these regularity conditions, Geroliminis and Daganzo (2008) showed that such a relationship existed in Yokohama. This relationship has come to be known as the ‘Macroscopic Fundamental Diagram’ (MFD).

More recent work (Buisson and Ladier, 2009) used empirical data to create an MFD plot of the Toulouse, France traffic network. Figure 1 displays the MFD’s of both Yokohama and Toulouse for comparison. Notice that all observations in the Yokohama dataset fall approximately along the same curve, with only a single value of flow for each density. However, the Toulouse observations of June 13, 2008, which are magnified with time stamps in the inset of the figure, exhibit multiple flow values for some densities. In fact, there appears to be a clockwise hysteresis-like loop with higher flows as the density increases and lower flows as the density decreases. It was noted in Buisson and Ladier (2009) that on this particular day a social movement of truck drivers reduced speeds and created congestion on the ring road surrounding the city between 8 AM and 10 AM, causing drivers to change routes. The lower flows were attributed to the non-homogeneous congestion in the network created by this disturbance.

This explanation seems reasonable since a major disturbance can distribute traffic unevenly in space, and it is well known that uneven vehicle distributions can reduce flow (Daganzo, 2007; Daganzo and Geroliminis, 2008). What is still puzzling, however, is why low flows are only observed when the network is recovering from congestion (from 9 AM to sometime after 11 AM)—long after the disturbance started—and why the low flows persist well after the disturbance ended.

An explanation may lie in recent computer simulations which show that traffic congestion tends to distribute itself unevenly when a fixed number of drivers are forced to circulate in a network indefinitely while choosing their routes randomly (Daganzo et al., 2010; Gayah and Daganzo, 2010; Mazlounian et al., 2010). Daganzo et al. (2010) shows with an analytical model of a simple network consisting of two bins that the ultimate reason for this phenomenon is turning at intersections: random turns cause congested regions to attract more traffic than they emit, misdistributing congestion. This reference also shows that if drivers choose their routes adaptively in real-time then the tendency toward unevenness is mitigated, albeit not completely if congestion is heavy. If this tendency toward unevenness also arises for more realistic scenarios in which drivers are allowed to enter and exit a network according to their wishes, it could explain the delayed hysteresis pattern observed in Toulouse. The pattern could be due to a gradual buildup of congestion unevenness that became self-sustained once it started.

To look into this issue, this paper generalizes the simple two-bin model in Daganzo et al. (2010) to account for the dynamics of a rush hour. This model will be used to see if the observations in Buisson and Ladier (2009) can be qualitatively reproduced, and to shed light on when and how hysteresis arises. It will be assumed that trip generation is time-dependent and exogenous, but the trip termination rate is endogenous. The latter is assumed to be proportional to the circulating

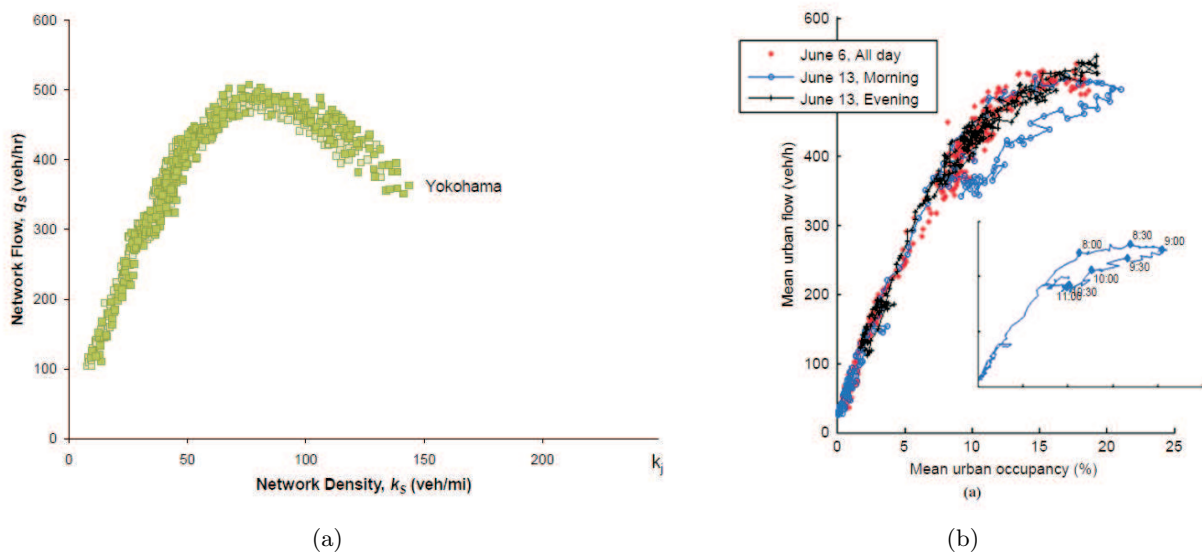


**Figure 1.** Empirical MFDs of: (a) Yokohama, Japan; and (b) Toulouse, France (source: Buisson and Ladier, 2009)

flow as recommended in the literature (Daganzo, 2007; Geroliminis and Daganzo, 2008).

It is found that hysteresis loops do arise. It is also found that a network’s tendency toward unevenness is exacerbated during the late stages of a rush hour when more trips are terminating than starting, especially if drivers do not navigate through congestion adaptively, and this causes hysteresis loops to follow a clockwise pattern. In other words, the dynamics of (exogenous) network loading and (endogenous) network recovery are asymmetric. This helps explain why the Toulouse observations only exhibit low flows during recovery on a day when many drivers were forced into unfamiliar routes.

The paper is organized as follows. Section 2 describes the simple two-bin network. Section 3 presents its dynamic equations assuming no driver adaptation, and explores the asymmetry between the beginning of a rush hour (loading) and its end (recovery). Section 4 examines full rush hour cycles and the conditions giving rise to hysteresis loops of different types. Section 5 examines driver adaptation and the behavior of real traffic networks.

## 2 The Simple Network: A Two-Bin System

The two-bin system used in Daganzo et al. (2010) to model a homogeneous square grid network will also be used here. Whereas each of the bins in this reference represented a family of parallel streets, here they will represent adjacent neighborhoods, as illustrated by the dotted rectangles in Figure 2(a). Each of these rectangular neighborhoods can be modeled as a bin of vehicles with an MFD if traffic within it can be assumed to be uniformly distributed in space.

In view of this, the network is idealized as depicted in Figure 2(b). The density of vehicles within each bin is denoted  $k_i$  [veh/km], where  $i = 1$  or  $2$ . In order not to introduce confounding factors, it is assumed that the bins are completely symmetric in that: (i) they have identical network lengths,  $L$  [km], and (ii) the circulating flow within each bin,  $q_i$  [veh/hr], is described by the same MFD,  $q_i = Q(k_i)$ . The MFD of each bin is assumed to be triangular as illustrated in Figure 3. The flow of vehicles turning out of each bin (and into the other),  $f_i$  [veh/hr], is defined as a constant fraction,

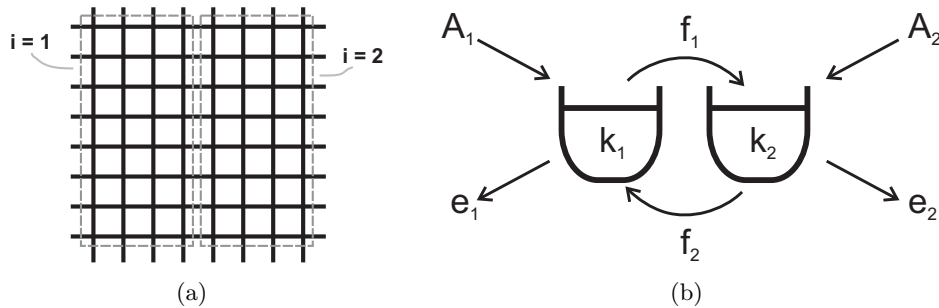


**Figure 2.** (a) Neighborhoods within a city network; and (b) a two-bin idealization.

$P_T$ , of the circulating flow within each bin; therefore,  $f_i = P_T Q(k_i)$  as in Daganzo et al. (2010). Finally, it is assumed that the receiving bin has sufficient capacity to absorb the turning flow from the sending bin unless the receiving bin is completely filled with vehicles.<sup>1</sup>

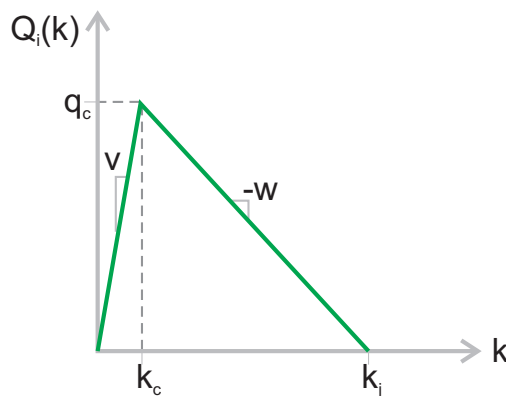


**Figure 3.** Triangular bin MFD.

In addition to these circulating rules, each bin experiences a constant inflow  $A_i$  [veh/hr], and a state-dependent variable outflow  $e_i$  [veh/hr]. This outflow is assumed to be a fixed proportion,  $P_E$ , of the circulating flow as recommended in Daganzo (2007) and Geroliminis and Daganzo (2008). Therefore,  $e_i = P_E Q(k_i)$ .

## 2.1 State Space and Flow-Density Relationship of the Two-Bin System

The state of the system is the density pair  $(k_1, k_2)$ . This state describes the traffic conditions in the two bins. For any  $(k_1, k_2)$  pair, the system's average density is:

$$k_S = \frac{k_1 L + k_2 L}{2L} = \frac{k_1 + k_2}{2}, \quad (1a)$$

and the system's average flow is:

$$q_S = \frac{q_1 L + q_2 L}{2L} = \frac{q_1 + q_2}{2} = \frac{Q(k_1) + Q(k_2)}{2}. \quad (1b)$$

<sup>1</sup>It was shown in Daganzo et al. (2010) that this simplification does not significantly affect the qualitative behavior of the model.

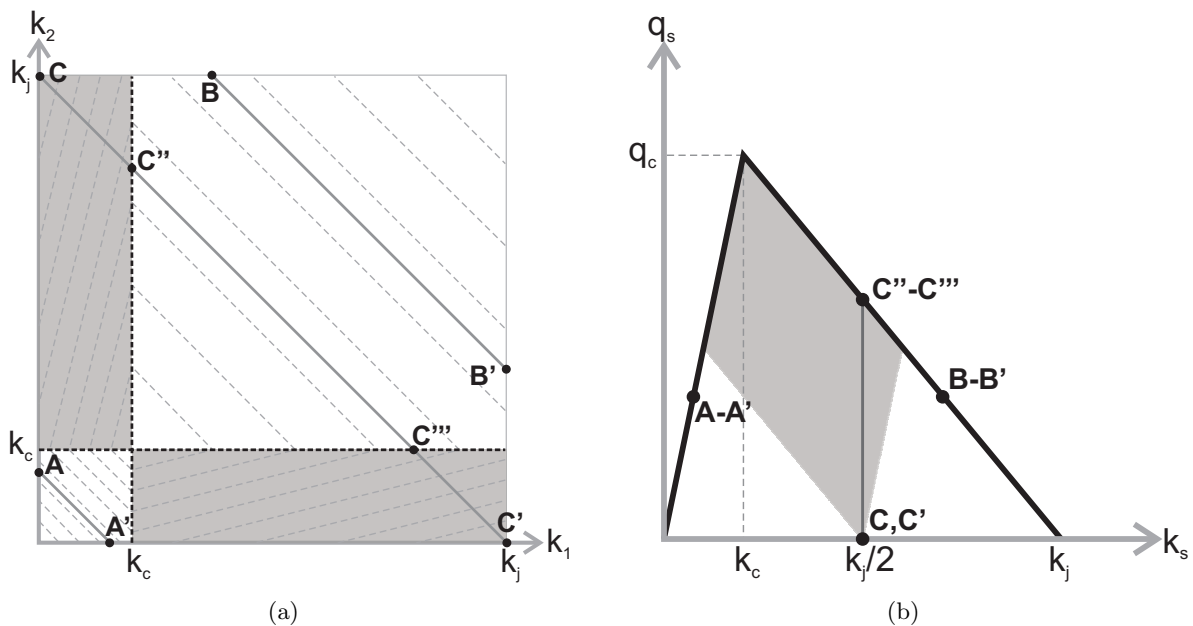


**Figure 4.** (a) Phase diagram displaying the state-space of the two-bin system; (b) plot of system flow ( $q_s$ ) vs. system density ( $k_s$ ) in relation to MFD.

All possible states can be displayed graphically on a phase diagram such as the one in Figure 4(a). At any given time the system can exist in one of three possible regimes based on the traffic conditions in the two bins. These regimes are shaded differently in Figure 4(a), and are separated by horizontal and vertical dotted lines. The first regime (bottom-left quadrant) is the **Free-Free** or FF regime because both bins operate in free flow conditions. The second (top-right quadrant) is the **Congested-Congested** or CC regime because both bins are congested. The last regime (the shaded area) is the **Free-Congested** or FC regime because one bin operates in free flow and the other in congestion.

Equi-flow contours are also plotted on Figure 4(a) as dashed gray lines. Contour flows increase towards the interior where they take the form of trapezoids. Three equi-density contours are also shown: segments  $\overline{AA'}$ ,  $\overline{BB'}$ , and  $\overline{CC'}$ . These two sets of contours define a mapping from the phase diagram to the flow-density plane:  $(k_1, k_2) \rightarrow (k_s, q_s)$ ; see Figure 4(b). Consideration shows that the two quadrants representing the FF and CC regimes are mapped into the dark MFD triangle. This is a surjective mapping in which constant-density segments such as  $\overline{AA'}$ ,  $\overline{BB'}$ , and  $\overline{C''C''''}$  are mapped into points. Thus, a closed loop on the phase diagram contained strictly within one of these two regimes will be invisible on the flow-density plane, appearing as a line segment along the MFD.

In contrast, points in each of the rectangles representing the FC regime map one-to-one with points in the shaded parallelogram on the flow-density plane. (Figure 4 shows how segments  $\overline{CC''}$  and  $\overline{C''''C'}$  are mapped into another segment.) Thus, a closed loop on the phase diagram contained entirely within one of these rectangles will appear as a loop inside the shaded area of the flow-density plane. It is within this region that hysteresis will be observed for the two-bin system.



### 3 System Dynamics

The dynamic equations of the two-bin system are:

$$\begin{aligned} \frac{dk_1}{dt} &= \frac{A_1 - P_E Q(k_1) + P_T [Q(k_2) - Q(k_1)]}{L} \text{ and} \\ \frac{dk_2}{dt} &= \frac{A_2 - P_E Q(k_2) + P_T [Q(k_1) - Q(k_2)]}{L}, \text{ if } k_1, k_2 < k_j; \text{ and,} \end{aligned} \quad (2a)$$

$$\frac{dk_1}{dt} = \frac{dk_2}{dt} = 0, \text{ if } k_1 \text{ or } k_2 = k_j. \quad (2b)$$

These equations are now examined to understand how the system evolves during an idealized rush hour. Section 3.1 describes the evolution of the system when input flows are positive and exiting flows are zero (mimicking the beginning of a rush hour), and Section 3.2 the case when input flows are zero and exiting flows are positive (mimicking the end of a rush hour). The case when both input flows and exiting flows are positive is discussed in Appendix A.

#### 3.1 The Loading Process

Here  $A_i > 0$  ( $i = 1, 2$ ) and  $P_E = 0$ . To get to the heart of the issue, the behavior of the system is examined when it is loaded evenly (i.e.,  $A_1 = A_2 = A$ ) from different starting points. Furthermore, it will be convenient to denote the densities of the less loaded and more loaded bin by  $k$  and  $K$ , respectively. In this case, Equation (2a) simplifies to:

$$\frac{dk}{dt} = \frac{A + P_T [Q(K) - Q(k)]}{L} \text{ and } \frac{dK}{dt} = \frac{A + P_T [Q(k) - Q(K)]}{L}, \text{ if } k, K < k_j. \quad (3)$$

We are interested in determining whether the system converges to or diverges from a balanced state, i.e., the diagonal in Figure 5 for which  $k = K$ , as time passes. This is equivalent to determining if  $d(k - K)/dt$  is positive or negative. The reader can verify by subtracting both instances of (3) that:

$$\frac{d(k - K)}{dt} = \frac{2P_T}{L} [Q(K) - Q(k)], \quad (4)$$

and by adding both instances of (3) that:

$$\frac{dk_S}{dt} = \frac{A}{L}. \quad (5)$$

This last equation merely confirms that the system's average density increases with time at an exogenously fixed rate. Since density increases with time, a time-independent measure  $\tau$  describing the tendency of the system to converge to or diverge from a balanced state is the rate at which the system's balance changes with (increasing) density; i.e., the ratio of (4) and (5):

$$\tau \doteq \frac{d(k - K)}{dk_S} = \frac{2P_T}{A} [Q(K) - Q(k)], \text{ when } P_E = 0. \quad (6)$$

Note the system converges in time toward a balanced state if  $\tau > 0$  and diverges if  $\tau < 0$ ; i.e., it converges if  $Q(K) > Q(k)$  and diverges if  $Q(K) < Q(k)$ . These areas of convergence and divergence are displayed in Figure 5 as the C-area and the D-area, respectively. Note from (6) that the magnitude of the convergence measure depends on the ratio  $P_T/A$ ; the slower the loading and

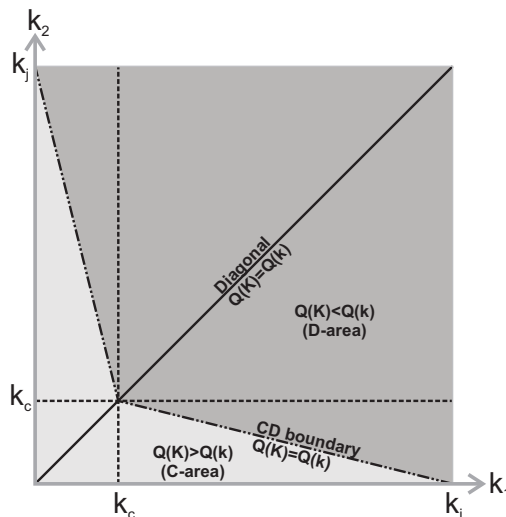


**Figure 5.** Areas of convergence to and divergence from equally loaded bins.

the greater the turns, the greater the tendency to converge or diverge.<sup>2</sup>

Figure 6(a) presents the evolution of the system on the phase diagram for various starting points according to (3); these lines are known as ‘loading paths’. As indicated by (6), the loading paths converge upon the diagonal when in the C-area and diverge away from it in the D-area. Also expected from (3) and (6) is that if the system starts from a balanced state, it will remain balanced throughout the loading process. Moreover, if it starts unbalanced it remains unbalanced and can never reach the diagonal. Note too that individual paths are closest to the diagonal when they cross the CD boundary, which is the locus of points in which  $Q(K) = Q(k)$ .

The converging and diverging behavior of the system during loading is caused by the turning that occurs between the two bins. If turning is non-existent ( $P_T = 0$ ) then  $\tau = 0$  and  $(k_1, k_2)$  would increase with time at the same fixed rate for both bins, and the difference  $(k - K)$  would remain constant. Loading paths for this special case are presented in Figure 6(b).

### 3.2 The Recovery Process

Considered here is the evolution of the system when vehicles exit the system without any input flows ( $A = 0$ ). In this case, (2a) becomes:

$$\frac{dk}{dt} = \frac{P_T Q(K) - (P_T + P_E)Q(k)}{L} \quad \text{and} \quad \frac{dK}{dt} = \frac{P_T Q(k) - (P_T + P_E)Q(K)}{L}. \quad (7)$$

Again, subtracting and adding both instances of (7) one finds that:

$$\frac{d(k - K)}{dt} = \frac{2P_T + P_E}{L} [Q(K) - Q(k)], \quad (8)$$

and:

$$\frac{dk_S}{dt} = -\frac{P_E q_S}{L}. \quad (9)$$

These expressions are very similar to (4) and (5), except now  $dk_S/dt$  is negative. The average

<sup>2</sup>The same type of analysis reveals that if entering flows were endogenously determined, recognizing that fewer vehicles may be able to enter a more congested bin, then the system would have an even greater tendency to converge towards a balanced equilibrium.

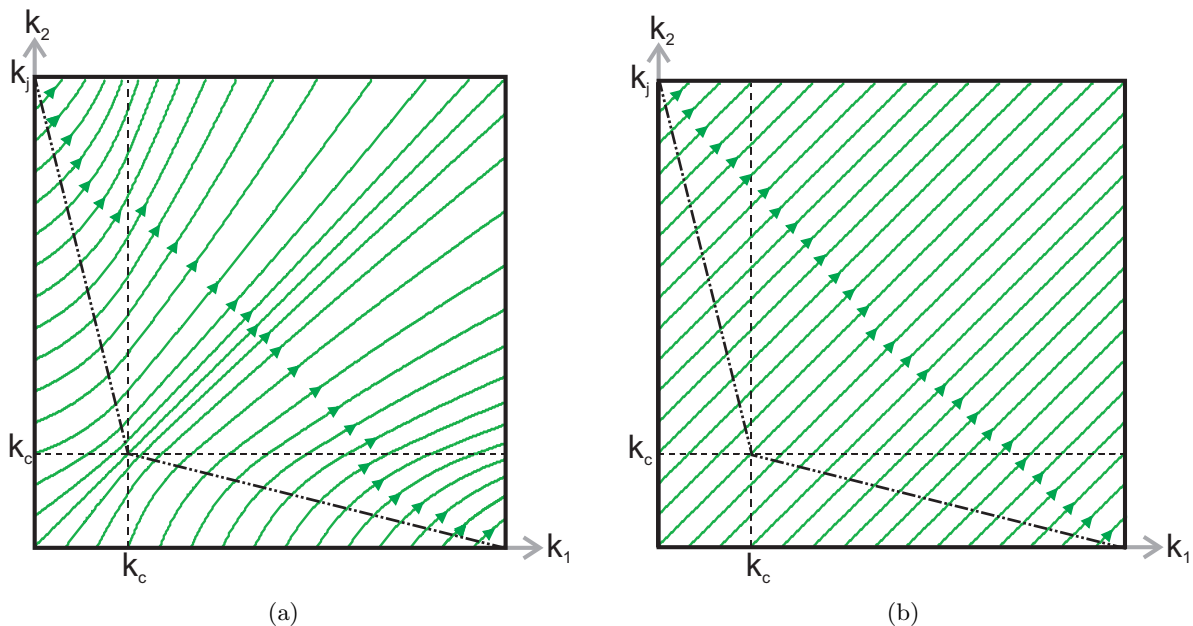


**Figure 6.** Loading paths for  $A = 0.2q_c$  and: (a)  $P_T = 0.05$ ; and (b)  $P_T = 0.0$ .

density of the system now decreases with time at a rate that is a constant proportion of the circulating flow. In view of this, the time-independent convergence measure during recovery is defined as  $\tau' \doteq -d(k - K)/dk_S$ , which on dividing (8) and (9) reduces to:

$$\tau' \doteq -\frac{d(k - K)}{dk_S} = \frac{2P_T + P_E}{P_E q_S} [Q(K) - Q(k)], \text{ when } A = 0. \quad (10)$$

Note the only difference between (6) and (10) is the coefficient of  $[Q(K) - Q(k)]$ . Thus during recovery the system has the same C- and D-areas; see Figure 5. The coefficient  $(2P_T + P_E)/(P_E q_S)$  shows that the greater the turns and the lesser the exiting traffic, the greater the tendency to converge or diverge.<sup>3</sup>

The shape of recovery paths is different from the shape of the loading paths because the coefficient is now state-dependent; Figure 7(a) shows some examples. Of course, the direction of these paths is reversed from those of Figure 6(a) because the sign of (9) is different from that of (5). As in the loading case, if the system starts recovering from a balanced state, it remains balanced throughout recovery, and if it starts unbalanced it remains unbalanced. Unlike in the loading case, however, the recovery paths cross the CD boundary when they are farthest from the diagonal, and not at their closest. Thus, if the system begins recovery from an unbalanced state in the D-area, the unevenness grows until the phase path crosses the CD boundary and enters the C-area.

Another key difference between loading and recovery can be observed by setting  $P_T = 0$ . In this case,  $\tau' \neq 0$  if  $Q(K) \neq Q(k)$ , but 6 shows that  $\tau = 0$  for the loading process. Thus, during recovery, but not during loading, congestion unevenness increases while the system is in the D-area and decreases while in the C-area. The physical reason for this phenomenon is that with endogenous turning flows less congested areas clear more quickly than more congested areas. In contrast, with exogenous input flows, congestion builds up evenly during loading. This is why the recovery process is inherently more unstable than the loading process. Consideration of 10 shows

<sup>3</sup>The limit case with  $P_E = 0$  yields  $\tau' = \pm\infty$ . This means that if  $k_S$  is held fixed then the phase paths are perpendicular to the diagonal, in agreement with the model in Daganzo et al. (2010).

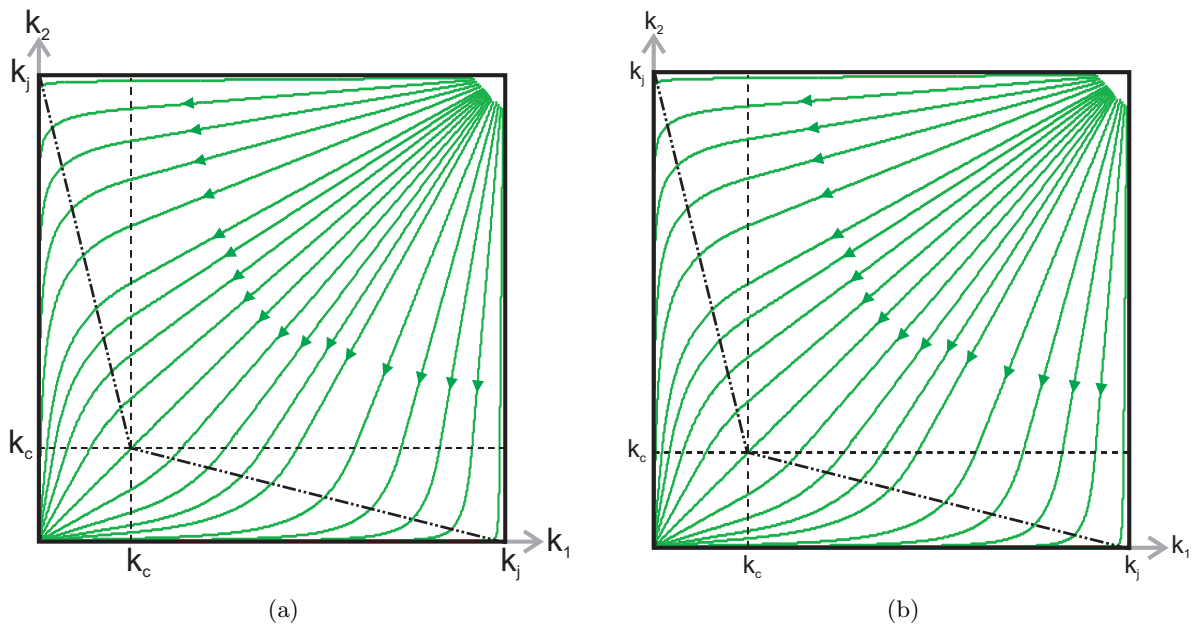


**Figure 7.** Recovery paths for  $P_E = 0.2$  and: (a)  $P_T = 0.05$ ; and (b)  $P_T = 0.0$ .

that the presence of turning exacerbates this effect.

## 4 Hysteresis Loops in the MFD

It is clear from Sections 3.1 and 3.2 that loading and recovery paths are asymmetric. The translation of these paths from the phase diagram to the flow-density plane is now examined to see what types of patterns emerge due to this asymmetric behavior, and the conditions that define each pattern. To do this, the evolution of the system during a loading/recovery (LR) cycle is studied. An LR cycle has two phases: a loading phase with  $A > 0$  and  $P_E = 0$ , starting from some initial state in the FF regime  $(k_1^o, k_2^o)$ , until it reaches a maximum density  $k_S^*$ ; and a recovery phase with  $A = 0$  and  $P_E > 0$  that lasts until the system is completely empty. These LR cycles are used for analysis because they can mimic a variety of idealized rush hour periods by varying only three parameters—the initial starting point  $(k_1^o, k_2^o)$  and the final density  $k_S^*$ . Four different types of patterns are discovered: single-path, clockwise hysteresis loops, counter-clockwise hysteresis loops, and figure-eight patterns; see Figure 8.

single-path patterns exhibit the same flows for the same density during the loading and recovery phases, and all data points lie on the MFD. Recall from Section 2.1 that this pattern can only occur if the system stays in the FF and/or CC regimes during the LR cycle. This can happen in only two ways: either  $(k_1^o, k_2^o)$  is balanced, in which case the system stays balanced, or else the final state with density  $k_S^*$  is in the FF regime so that the phase path is entirely contained within the FF regime.

Clockwise hysteresis loops exhibit higher flows as the system density increases than as it decreases. Since lower flows are observed as the system becomes more unbalanced, clockwise loops only occur when the system recovers along a phase path that is further away from the diagonal than the path on which it was loaded. This occurs if  $(k_1^o, k_2^o)$  is moderately unbalanced so that the path taken during loading is near the diagonal, and  $k_S^*$  is so high that the system recovers along a more eccentric path. These conditions are easy to meet; thus, clockwise loops should be common.

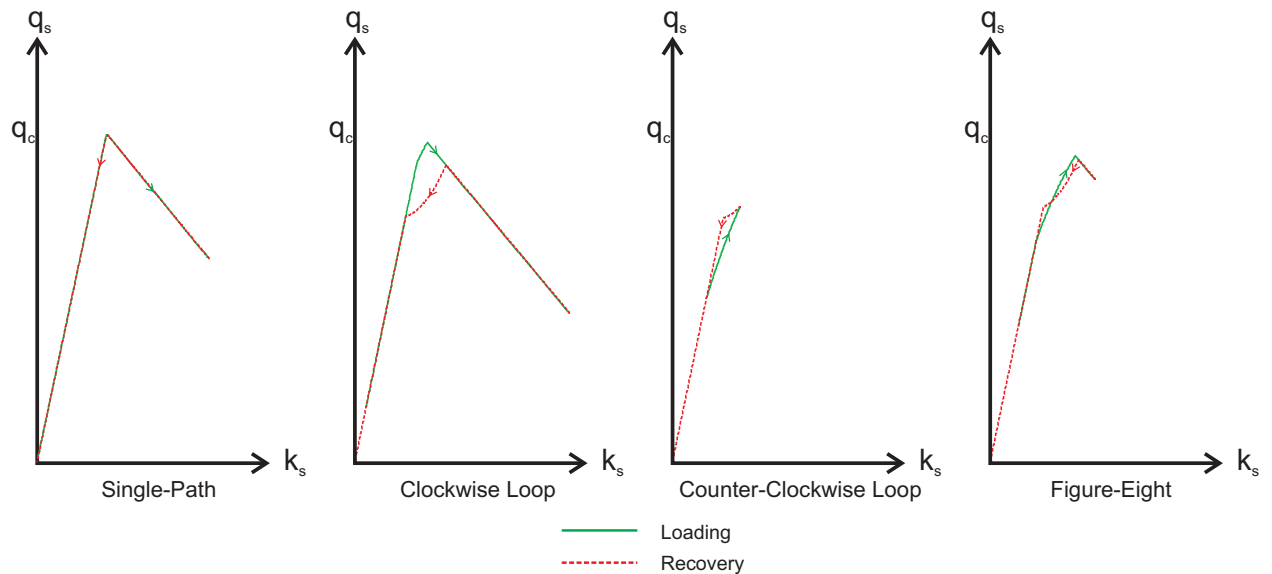


**Figure 8.** Types of patterns observed on the flow-density plane.

Counter-clockwise loops exhibit lower flows as the system density increases than as it decreases. These loops can only be observed if the system recovers along a phase path closer to the diagonal than the path on which it was loaded. This can only occur if  $(k_1^o, k_2^o)$  is very unbalanced so that the path taken during loading is far from the diagonal and  $k_S^*$  is so low that the system enters the FC regime without penetrating the D-area. This should be rare.

Figure-eight patterns are a combination of both clockwise and counter-clockwise loops—observed flows are higher during loading for high densities and lower during loading for low densities. This pattern occurs when the path taken during recovery crosses the path taken during loading in the FC regime. This occurs if  $(k_1^o, k_2^o)$  is very unbalanced and  $k_S^*$  is very high. These conditions are also rare, but not as much as those for counter-clockwise loops.

## 5 More Realistic Driver Behavior

It was previously assumed that drivers followed predetermined and deterministic routes so that  $P_T$  was fixed in the two-bin model. These assumptions are now relaxed. Section 5.1 examines the effects of driver adaptivity to real-time congestion in the two-bin model, and Section 5.2 discusses more realistic networks.

### 5.1 Driver Adaptivity

It is possible that drivers who adapt to congestion within the network may help eliminate or reduce the hysteresis loops that are observed when drivers behave rigidly. To study the effect of adaptive drivers systematically with the two-bin model, it is now assumed that some proportion,  $\alpha$ , of the drivers are ‘adaptive’ and will not turn from a less congested bin into a more congested one. With this modification, the dynamic equations for the system during the loading process (now written in terms of  $k$  and  $K$ ) become:

$$\frac{dk}{dt} = \frac{A + P_T Q(K) - (1 - \alpha) P_T Q(k)}{L} \quad \text{and} \quad \frac{dK}{dt} = \frac{A + (1 - \alpha) P_T Q(k) - P_T Q(K)}{L}, \quad (11)$$

and the convergence measure for loading changes to:

$$\tau = \frac{d(k - K)}{dk_S} = \frac{2P_T}{A}[Q(K) - (1 - \alpha)Q(k)]. \quad (12)$$

Examination of (12) shows that during loading the system converges towards a balanced state when  $Q(K) > C_L Q(k)$  and diverges away from it when  $Q(K) < C_L Q(k)$ , where  $C_L = 1 - \alpha$ . The C-area and D-area for  $C_L = 0.8$  are plotted in Figure 9. The C-area grows and the D-area shrinks as  $\alpha$  increases and drivers become more adaptive. Furthermore, (12) is monotonically increasing with  $\alpha$ . Thus, the tendency toward evenness increases with the adaptivity of the drivers.

The dynamic equations during the recovery process when drivers are adaptive are:

$$\frac{dk}{dt} = \frac{P_T Q(K) - ((1 - \alpha)P_T + P_E)Q(k)}{L} \quad \text{and} \quad \frac{dK}{dt} = \frac{(1 - \alpha)P_T Q(k) - (P_T + P_E)Q(K)}{L}, \quad (13)$$

and the convergence measure changes to:

$$\tau' = -\frac{d(k - K)}{dk_S} = \frac{1}{P_E q_S} [(2P_T + P_E)Q(K) - (2(1 - \alpha)P_T + P_E)Q(k)]. \quad (14)$$

Examination of (14) shows that during recovery the system converges towards a balanced state when  $Q(K) > C_R Q(k)$  and diverges away from it when  $Q(K) < C_R Q(k)$ , where  $C_R = 1 - 2\alpha P_T / (2P_T + P_E)$ . Note that if  $C_L = C_R$  the C- and D-areas are the same for both recovery and for loading. Thus, Figure 9 also presents the C- and D-area for  $C_R = 0.8$ . As with the loading process, the C-area grows and the D-area shrinks as drivers become more adaptive, and because (14) continues to be monotonically increasing with  $\alpha$  the tendency towards evenness continues to increase with the adaptivity of the drivers. For a given value of  $\alpha$ ,  $C_L \leq C_R$ , however; therefore, the system will tend toward balance more strongly during loading than during recovery.

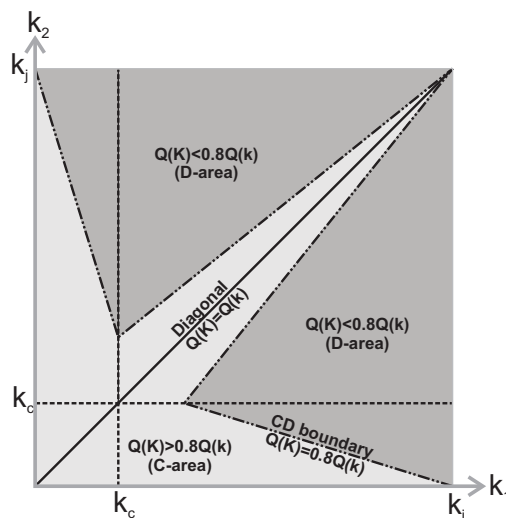


**Figure 9.** Areas of convergence to and divergence from equally loaded bins when drivers are adaptive for  $C_L = 0.8$  (loading) and  $C_R = 0.8$  (recovery).

Sample loading and recovery paths are presented in Figure 10. Unlike in the non-adaptive case, loading paths and recovery paths that start at some unbalanced states are now able to reach the diagonal. Thus, it is now possible for a single-path pattern along the MFD to occur during a LR cycle even when the two-bin system starts out of balance. The range of starting states that

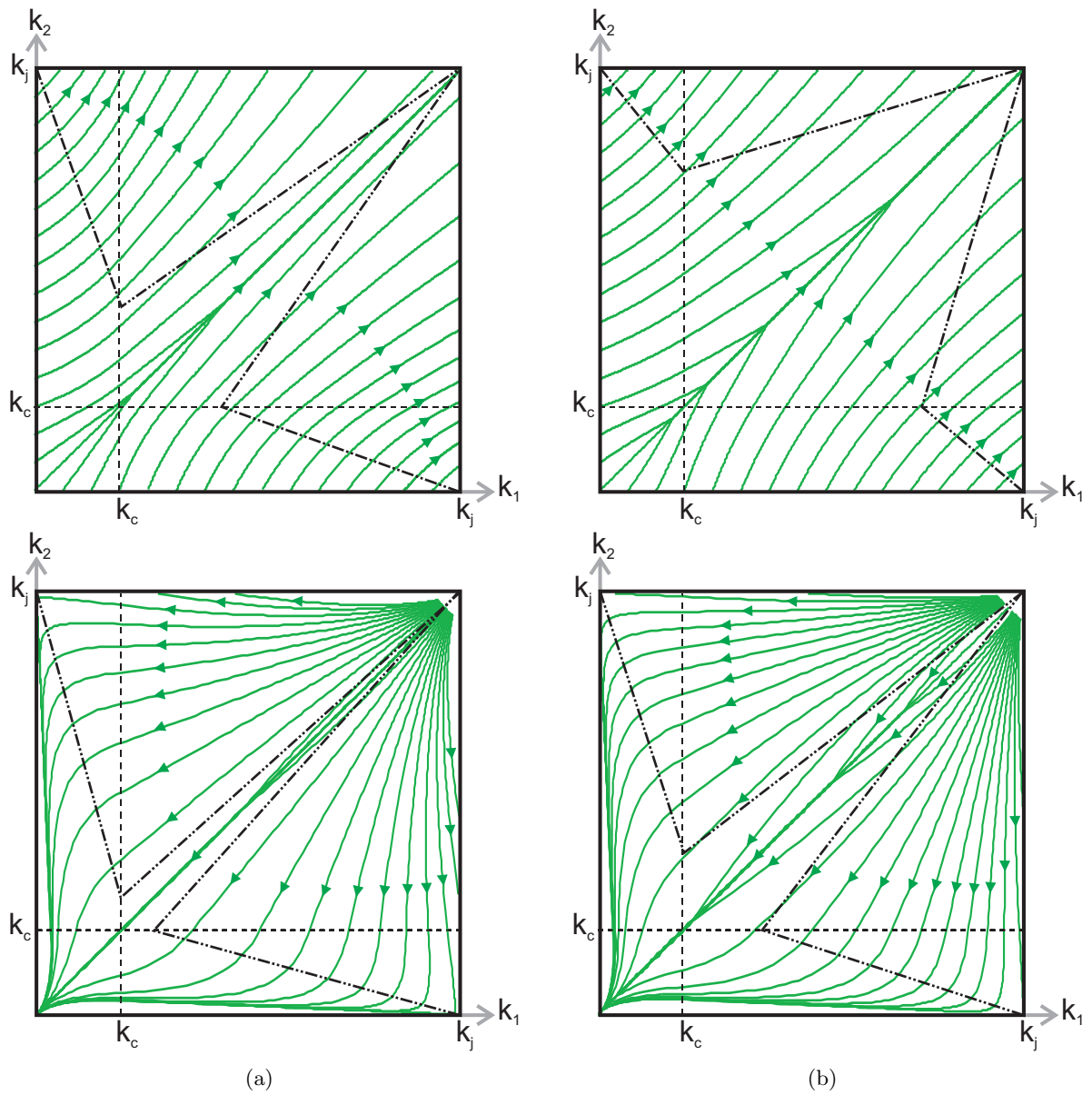


**Figure 10.** Loading paths (top) and recovery paths (bottom) for two adaptation levels: (a)  $\alpha = 0.3$ ; and (b)  $\alpha = 0.7$ . In all cases  $A = 0.2q_c$ ,  $P_E = 0.2$ , and  $P_T = 0.05$ .

converge to the diagonal during loading and recovery increases with the level of driver adaptivity. Therefore, the probability of observing the single-path regime increases (and the probability of observing hysteresis loops decreases) with the adaptivity of the drivers.

This behavior is also observed when the rate of turning between the two bins is not deterministic but instead is allowed to fluctuate randomly around  $P_T Q(k_i)$ . In this case, the starting state  $(k_1^o, k_2^o)$  is less important as random variations in the turning flows cause the system's balance to jump around. Sample phase paths are displayed in Figures 11(a) and 11(b) for  $\alpha = 0.7$  and  $\alpha = 0.3$ , respectively, for LR cycles that begin with the system completely empty. Note from this figure that when drivers are very adaptive, imbalances in the system tend not grow; phase paths stay close to diagonal and single-path patterns are observed on the flow-density plane. When drivers are less adaptive, small imbalances in the system grow, and clockwise hysteresis loops arise.

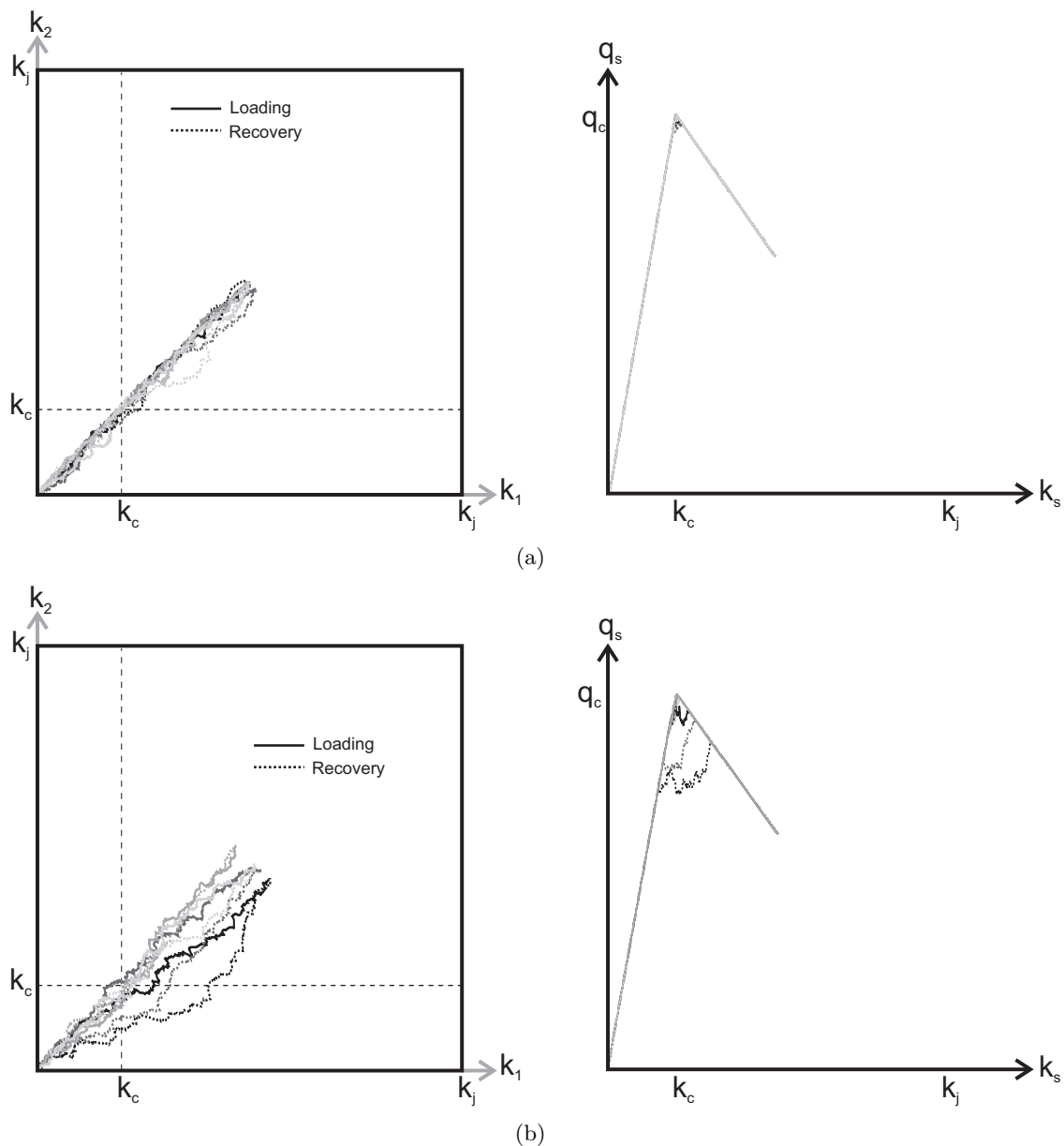


**Figure 11.** Phase paths with random turns,  $A = 0.2q_c$ ,  $P_T = 0.05$ ,  $P_E = 0.2$ , loading period of 500 time-steps,  $(k_1^o, k_2^o) = (0, 0)$  and: (a)  $\alpha = 0.7$ ; and (b)  $\alpha = 0.3$ . (What appear to be portions of a triangle are actually sample paths in the CC regime.)



## 5.2 More Realistic Networks

The qualitative behavior of the two-bin system studied in this paper can be extended to more realistic traffic networks since real traffic networks can be modeled as a similar system consisting of many more bins. These multiple bin systems are not studied here because their qualitative behavior should not be too different. Although it is very unlikely that all bins in such a system would be congested simultaneously, we still expect two effects: (i) recovery to be more unstable than loading;<sup>4</sup> and (ii) this instability to increase with the lack of driver adaptation.

This is precisely what is seen in the Toulouse network. On the day of the truck strike drivers on the city streets must have become less adaptive, since some would have switched off of the ring road to unfamiliar routes, and a clockwise hysteresis loop was observed. As in the two-bin simulations, in Toulouse low flows were mainly observed during recovery and the hysteresis loop continued until the end of the rush. Effect (i) is perhaps why low flows were observed only when the network was recovering from congestion resulting in a clockwise loop, and effect (ii) why this only happened on the day of the truck strike. Effects (i) and (ii) combined explain why these low flows continued after the truck strike ends.

On the other days, hysteresis loops are not observed perhaps because driver adaptivity is very high. High driver adaptivity probably also explains why no hysteresis loops exist in Yokohama. We would expect the Yokohama network to exhibit a clockwise hysteresis loop if it was subjected to a disturbance similar to that of Toulouse. More empirical data from surface networks is of course necessary to verify or disprove the conjectures in this paper.

The results of the two-bin model also suggest that MFD hysteresis loops should be very likely on freeway systems because the topology of these systems gives drivers fewer opportunities to adapt. Recent experimental data indeed confirms the presence of MFD hysteresis loops on freeway systems (Geroliminis and Sun, 2010). Since freeway data are plentiful, and freeway systems are simpler than urban networks, it may be possible to investigate the former with a more realistic model than the two-bin network. This could yield additional insights which could be tested with real data.

## Acknowledgments

This research was supported by NSF Grant CMMI-0856193 and the UC Berkeley Center of Excellence for Future Urban Transport.

---

<sup>4</sup>The reason is that (as in the two-bin model) congested portions of the network can discharge vehicles less rapidly than those less congested.

## References

- Ardekani, S. and Herman, R. (1987). Urban network-wide traffic variables and their relations. *Transportation Science*, 21(1):1–16.
- Buisson, C. and Ladier, C. (2009). Exploring the impact of homogeneity of traffic measurements on the existence of macroscopic fundamental diagrams. *Transportation Research Record: Journal of the Transportation Research Board*, 2124:127–136.
- Daganzo, C. (2007). Urban gridlock: Macroscopic modeling and mitigation approaches. *Transportation Research Part B*, 41(1):49–62.
- Daganzo, C., Gayah, V., and Gonzales, E. (2010). Macroscopic relations of urban traffic variables: Bifurcations, multivaluedness and instability. *Transportation Research Part B*, doi:10.1016/j.trb.2010.06.006.
- Daganzo, C. F. and Geroliminis, N. (2008). An analytical approximation for the macroscopic fundamental diagram of urban traffic. *Transportation Research Part B*, 42(9):771–781.
- Gayah, V. V. and Daganzo, C. (2010). Exploring the effect of turning maneuvers and route choice on a simple network. *UC Berkeley, Volvo Working Paper UCB-ITS-VWP-2010-05*.
- Geroliminis, N. and Daganzo, C. F. (2008). Existence of urban-scale macroscopic fundamental diagrams: Some experimental findings. *Transportation Research Part B*, 42(9):759–770.
- Geroliminis, N. and Sun, J. (2010). Properties of a well-defined macroscopic fundamental diagram for urban systems. In *Compendium of papers CD-ROM, Transportation Research Board 89th Annual Meeting, Washington DC*, number 10-3521.
- Godfrey, J. (1969). The mechanism of a road network. *Traffic Engineering and Control*, 11(7):323–327.
- Herman, R. and Prigogine, I. (1979). A two-fluid approach to town traffic. *Science*, 204(4389):148–151.
- Mahmassani, H. and Peeta, S. (1993). Network performance under system optimal and user equilibrium dynamic assignments: Implications for advanced traveler information systems. *Transportation Research Record*, 1408:83–93.
- Mazlounian, A., Geroliminis, N., and Helbing, D. (2010). The spatial variability of vehicle densities as determinant of urban network capacity. *Philosophical Transactions for the Royal Society A*, doi:10.1098/rsta.2010.0099.
- Olszewski, P., Fan, H., and Tan, Y. (1995). Area-wide traffic speed-flow model for the Singapore CBD. *Transportation Research Part A*, 29(4):273–281.

## Appendix A: Entering and Exiting Flows

The behavior of the system when vehicles enter and exit simultaneously is now examined to see if equilibrium states exist in which the density of the system does not change with time. Only the case with  $A_1 = A_2 = A$  is considered so (2a) becomes:

$$\begin{aligned} \frac{dk_1}{dt} &= \frac{A + P_T Q(k_2) - (P_T + P_E)Q(k_1)}{L} \text{ and} \\ \frac{dk_2}{dt} &= \frac{A + P_T Q(k_1) - (P_T + P_E)Q(k_2)}{L}, \text{ if } k_1, k_2 < k_j. \end{aligned} \quad (15a)$$

The sum of the two right-hand sides in (15) is  $(2A - P_E(Q(k_1) + Q(k_2)))/L$ , while their difference is  $(2P_T + P_E)(Q(k_2) - Q(k_1))/L$ . At equilibrium, both of these quantities have to be zero. Thus, an equilibrium with  $k_1, k_2 < k_j$  will only occur if the second quantity is zero, i.e.:

$$Q(k_1) = Q(k_2) \doteq Q; \quad (16a)$$

and if in addition the first quantity is zero, i.e.:

$$Q = A/P_E. \quad (16b)$$

Since  $Q \leq q_c$ , equilibrium solutions only exist for  $A/P_E \leq q_c$ .

Consideration shows that there are four  $(k_1, k_2)$  pairs that satisfy (16) for each value of  $Q < q_c$ : one in the FF regime, one in the CC regime, and one in each of the rectangles of Figure 4(a) representing the FC regime. The locus of all these equilibria for all  $Q \leq q_c$  turns out to be the union of the diagonal and CD boundary of Figure 5. These are the same equilibria found in Daganzo et al. (2010).

These equilibrium solutions  $(k_1^{eq}, k_2^{eq})$  are stable if and only if small perturbations to the equilibrium densities  $\epsilon_1$  and  $\epsilon_2$  shrink with time. Stable equilibria are important because the system tends towards them and they are reproducible. The reader can verify that (15) can be written in terms of the perturbations as follows:

$$\frac{d\epsilon_1}{dt} = \frac{P_T Q'(k_2^{eq})\epsilon_2 - P_T Q'(k_1^{eq})\epsilon_1 - P_E Q'(k_1^{eq})\epsilon_1}{L}, \quad (17a)$$

$$\frac{d\epsilon_2}{dt} = \frac{P_T Q'(k_1^{eq})\epsilon_1 - P_T Q'(k_2^{eq})\epsilon_2 - P_E Q'(k_2^{eq})\epsilon_2}{L}, \quad (17b)$$

which can be rewritten in matrix form as:

$$\begin{bmatrix} d\epsilon_1/dt \\ d\epsilon_2/dt \end{bmatrix} = \frac{1}{L} \begin{bmatrix} -(P_T + P_E)Q'(k_1^{eq}) & P_T Q'(k_2^{eq}) \\ P_T Q'(k_1^{eq}) & -(P_T + P_E)Q'(k_2^{eq}) \end{bmatrix} \begin{bmatrix} \epsilon_1 \\ \epsilon_2 \end{bmatrix} = \underline{\underline{M}} \underline{\epsilon}. \quad (18)$$

Clearly, the perturbations  $\underline{\epsilon}^{(1)}$  after a single time step,  $dt$ , are related to the initial perturbation  $\underline{\epsilon}^{(0)}$  by:

$$\underline{\epsilon}^{(1)} = [\underline{\underline{I}} + \underline{\underline{M}}dt] \underline{\epsilon}^{(0)}. \quad (19)$$

And, after  $n$  time steps the perturbations  $\underline{\epsilon}^{(n)}$  are:

$$\underline{\epsilon}^{(n)} = [\underline{I} + \underline{M}dt]^n \underline{\epsilon}^{(0)}. \quad (20)$$

Thus, the equilibrium is stable if and only if  $[\underline{I} + \underline{M}dt]^n \rightarrow \underline{0}$ ; i.e., if all the eigenvalues of  $[\underline{I} + \underline{M}dt]$  are less than one in absolute value. The reader can verify from (18) that all equilibria on the CD boundary and on the congested part of the diagonal are unstable. Only the portion of the diagonal in the FF regime is stable. This is different from the result in Daganzo et al. (2010), which found that solutions on the CD boundary were stable. The reason for this discrepancy is that in this reference exiting flows were exogenous, whereas here they are endogenous. This further illustrates the destabilizing effect of endogeneity.